Journal of Hydrology (2008) **360**, 132–146

available at www.sciencedirect.com

ScienceDirect

journal homepage: www.elsevier.com/locate/jhydrol

Analysis of runoff–storage relationships to evaluate the runoff-buffering potential of a sloping permeable domain

Makoto Tani *

Graduate School of Agriculture, Kyoto University, Kitashirakawa Sakyo Kyoto 606-8502, Japan

Received 24 March 2008; received in revised form 7 July 2008; accepted 17 July 2008

KEYWORDS
Macropores;
Rainfall-runoff response;
Richards equation;
Runoff-buffering potential;
Soil physical properties

Summary The runoff–storage relationship for a runoff system in a steady-state is analyzed as an indicator of the buffering potential of rainfall-runoff responses. In this relationship, a large storage increase in response to a given runoff increase indicates high buffering potential in the water balance equation. The evaluation method is applied to a sloping permeable domain. A two-dimensional form of the Richards equation is used to calculate runoff and storage. Macropore existence is represented by an enlargement effect of hydraulic conductivity near saturation. The runoff–storage relationship is controlled by the distribution of hydraulic quantities. The distribution of a pressure-head value is approximately classified into the following three zones: the I zone with vertical unsaturated flow, the U zone with unsaturated downslope flow, and the S zone with saturated downslope flow. The runoff-buffering potential is systematically evaluated by dependencies of the runoff–storage relationship on the classification of the pressure-head distribution. The potential is generally high for soil with a high permeability, but rather small in the range of low runoff rates where the S zone is not created. The macropore effect causes the range of high buffering potential to shift to high runoff rates through enlargement of the I zone. As a result, a moderate magnitude of the macropore effect gives the maximum increase in storage in response to a given increase in runoff.

Introduction

Although storm runoff is widely expected to decrease in forests (e.g., Bradshaw et al., 2007), this process has not been supported by many hydrological studies (Calder, 1999) and is a complex issue requiring further scientific examination. Forests may help mitigate the rainfall-runoff response through the formation of soil with large pores at a hillslope scale (e.g., Grip et al., 2004; Hayashi et al., 2006). Specifying the effect of each slope property on runoff mitigation remains a basic and significant theme of forest hydrology.

* Tel.: +81 75 753 6086; fax: +81 75 753 6149.
E-mail address: tani@kais.kyoto-u.ac.jp

0022-1694/$ - see front matter © 2008 Elsevier B.V. All rights reserved.
doi:10.1016/j.jhydrol.2008.07.023

Generally, various slope properties such as surface geology, soil properties, vegetation type, and topography influence rainfall-runoff responses. Surface geology seems to be a dominant factor. Shimizu (1980) demonstrated that mountainous catchments consisting of sedimentary rock in Japan had fluctuant runoff hydrographs, whereas catchments consisting of igneous rock produced stable runoff hydrographs. Holmes et al. (2002) also observed a strong dependency of flow–duration curves on geology in the United Kingdom. Such clear classifications by geology might be attributable to basic differences in the underground structure controlling the allocation of rainwater to various flow paths within the soil and permeable bedrock (Katsuyama et al., 2005; Kosugi et al., 2006). Almost certainly, geology mainly controls the runoff-buffering potential of mountainous catchments. The effects of other catchment properties may be secondary.

Nevertheless, assessing the effects of properties other than geology is important from a practical viewpoint because watershed management often requires information on the spatial distribution of runoff characteristics within geologically similar mountain ranges. However, because their effects are less dominant than those of geology, individual properties often show overlapping or counteracting influences on runoff responses, and specification of each influence is challenging. For example, Montgomery and Dietrich (2002) compared runoff responses in many small catchments and concluded that topographic slope was not sensitive to them. They reasoned that the insensitivity to slope resulted from the fact that the response timescale was controlled by vertical unsaturated flow instead of downslope flow. This suggests that a topographic property may produce different runoff-response tendencies for unsaturated and saturated water flows. Another example is the ambivalent effect of slope length on storm runoff responses. A study of storm runoff generation processes using a trench at the bottoms of a hillslope found that although only wetter downslope portions of a long slope generated runoff responses at early stages of a storm event, higher runoff peaks resulted from a shorter slope after large cumulative rainfall (>100 mm; Tani, 1997). This suggests that a long slope has higher runoff-buffering potential than a short slope when the runoff contribution area is fixed as the entire slope in the wettest condition. In drier conditions, however, the potential is lower in a long slope because its wetter downslope condition is derived from a larger upslope drainage area. This reflects the assumption of TOPMODEL (Beven and Kirkby, 1979). Therefore, the subtler effects of individual properties may be difficult to detect under typical field observations. This does not mean that field observation is worthless, but rather that researchers should recognize that ambivalent results are common.

To evaluate the effects of each catchment property on runoff responses, sensitivity analyses based on theoretical approaches can compensate for insufficient findings from field studies. Many findings have accumulated from theoretical studies (e.g., Freeze, 1972; Zaslavski and Sinai, 1981). For example, hillslope geometries such as convergent and divergent shapes have been assessed using the Boussinesq model based on hydraulic groundwater theory (Fan and Bras, 1998; Troch et al., 2003). Ogden and Watts (2000) analyzed soil water movement in a two-dimensional domain using the Richards equation. They showed that the timescale necessary to progress from an initial condition with a low water table to a steady-state in response to constant rainfall was controlled by the initial soil moisture conditions as well as the drainage ability of groundwater. Duffy (1996) analyzed the water balance equation of a runoff system and demonstrated that the rainfall-runoff responses were strongly controlled by dynamics of the saturated and unsaturated storage volumes. Kao et al. (2001) divided the unsaturated zone into two zones and emphasized the role of unsaturated flow in the horizontal water movement in a two-dimensional system. Lee (2007) showed that runoff recession characteristics were based on the runoff–storage relationship derived from saturated and unsaturated flows. It is possible to develop sensitivity analyses from these results, and we can emphasize an importance of the interaction between saturated and unsaturated zones. Note that although the above studies did address the effects of catchment properties on various kinds of indices characterizing runoff processes, they did not explicitly evaluate runoff-buffering potential.

Another problem in the assessment of runoff-buffering properties is related to the macropores involved in water movement in the soil. Many observational studies of hillslope hydrology have demonstrated that macropores have considerable influence on runoff responses (e.g., Smettem et al., 1991; Kitahara et al., 1994; Uchida et al., 2001). Because some of these studies have provided evidence for rapid downslope flow between the soil and bedrock interface (Anderson et al., 1997; Tani, 1997), one of the most important roles may be to lower the groundwater table by rapid downslope flow (Tsutsumi et al., 2005). This would influence the runoff-buffering potential, but such relationships have not yet been examined from this viewpoint.

Our purpose in this study is to propose a new method for evaluating the runoff-buffering potential of a sloping permeable domain. First, we consider the water balance equation for the domain and explain how the runoff-buffering potential can be basically represented by the runoff–storage relationship derived from the spatial distributions of hydraulic quantities in a steady-state. Next, three components of water flow within a sloping permeable domain are approximately classified to understand the dependence of the runoff–storage relationship on the distribution of hydraulic quantities. Finally, effects of soil physical properties and macropores on the buffering potential are evaluated based on the runoff–storage relationship.

Theory and methods

Runoff–storage relationship as an indicator of runoff-buffering potential

Runoff responses to rainfall in catchments are successfully simulated by storage-based runoff models such as the Tank model (Sugawara, 1995), TOPMODEL (Beven and Kirkby, 1979), and HYCYMODEL (Fukushima, 1988). The basic nature of rainfall-runoff responses may originate from a water balance equation with a functional relationship of runoff and storage

$$\frac{dV}{dt} = f - e - q, \quad (1)$$

$$V = V(q), \quad (2)$$

where q is the runoff rate, f is the rainfall rate, e is the evapotranspiration rate, and V is the water storage of a runoff system. Because the water balance equation (Eq. (1)) is accepted for any runoff system, the runoff response to rainfall for a given system is characterized by a runoff–storage relationship (Eq. (2)). Hence, it may be important to comprehensively parameterize the effects of runoff-system properties using this relationship. A typical example of this parameterization is the runoff–storage relationship of the saturated zone storage in TOPMODEL, which is derived from the spatial distribution of catchment topographic properties (Beven and Kirkby, 1979). To evaluate the effects of catchment properties on rainfall-runoff responses, previous studies have used various indicators such as the hydrograph shape (Fan and Bras, 1998), time to steady-state (Ogden and Watts, 2000), and flow duration curve (Shimizu, 1980; Holmes et al., 2002). Compared with these indicators, the runoff–storage relationship may have merit because it can be regarded as an intrinsic property of a runoff system independent of rainfall influences.

The evaluation method using the runoff–storage relationship can be applied to any runoff system, but one of the simplest is a one-dimensional vertical infiltration process in the permeable domain. Therefore, we first examine the runoff–storage relationship in a vertical column in response to rainfall with constant intensity. Because the rainfall rate equals vertical runoff flux in a steady-state, a column with a large increase in water storage in response to rainfall can be simply characterized as having high runoff-buffering potential. However, while a deeper soil column clearly has high buffering potential, soil physical properties also control that potential. Kosugi (1999) analyzed the influence of soil physical properties on the buffering potential using a one-dimensional form of the Richards equation. He represented the buffering potential by the difference in the soil water storage between the hydrostatic equilibrium before rainfall and the steady-state achieved by a continuous rainfall supply at a constant intensity. He then defined the difference as the water storage index and used this index to evaluate buffering potential.

Kosugi's (1999) approach can be applied to more complex runoff systems. However, the assumption of hydrostatic equilibrium as the initial condition may be inappropriate in general because runoff systems rarely reach this state. A quasi-steady-state, in which the distributions of hydraulic quantities are in steady states, may be a more acceptable condition for the runoff-recession stage of a runoff system, as assumed in TOPMODEL (Beven and Kirkby, 1979). Let us consider a cyclic process starting from a steady-state and returning to it through another steady-state to evaluate the runoff-buffering potential of a given system (the top figure of Fig. 1). Assume a runoff system A in a steady-state that yields a runoff rate per unit catchment area q_{cA} equal to the supplied constant rainfall rate f_1. If the supplied rainfall rate increases to a larger rate of f_2 at $t = t_1$, q_{cA} gradually increases and approaches f_2. After enough time, the system reaches another steady-state yielding a runoff rate of $q_{cA} = f_2$. If the rainfall rate decreases to f_1 at $t = t_2$ from the steady-state with $q_{cA} = f_2$, q_{cA} gradually decreases and returns to f_1 given sufficient time. The storage increase ΔV_A after the rainfall increase ($f_1 \rightarrow f_2$) indicated by the hatched area is equal to the storage decrease after the rainfall decrease ($f_2 \rightarrow f_1$), which is indicated by another hatched area in the top figure of Fig. 1, because both are calculated as the difference between total rainfall and total runoff in the water balance equation. This result is reflected in the runoff–storage relationship shown in the bottom part of Fig. 1. If we consider another runoff system B with a larger volume of storage increase than system A in response to the same increase in runoff rate from f_1 to f_2, both the increase and the decrease in runoff rate have a larger delay as shown in the upper figure. Therefore, the runoff-buffering potential can be represented by the functional relationship between the runoff rate and steady-state storage.

Fundamental equations

As the next simplest type of runoff system (Kosugi, 1999), we can consider a sloping permeable domain with a constant depth and homogeneous hydraulic properties. We can apply a two-dimensional form of the Richards equation for this domain, neglecting three-dimensional water movement. The origin is placed at the upslope end of the surface of the domain, and the x-axis and z-axis are positive in the horizontal and downward directions, respectively (Fig. 2). The water movement within the domain is described as

$$q_x = -K\left(\frac{\partial \psi}{\partial x}\right), \quad (3)$$

$$q_z = -K\left(\frac{\partial \psi}{\partial z} - 1\right), \quad (4)$$

$$\frac{\partial \theta}{\partial t} = C\frac{\partial \psi}{\partial t} = -\frac{\partial q_x}{\partial x} - \frac{\partial q_z}{\partial z}. \quad (5)$$

The Richards equation is substituted for (3) and (4) into (5) as

$$\frac{\partial \theta}{\partial t} = C\frac{\partial \psi}{\partial t} = \frac{\partial}{\partial x}\left(K\frac{\partial \psi}{\partial x}\right) + \frac{\partial}{\partial z}\left\{K\left(\frac{\partial \psi}{\partial z} - 1\right)\right\}, \quad (6)$$

where q_x and q_z are the water flow components in the x and z directions, respectively, K is the hydraulic conductivity, ψ is the pressure-head (the total water head of the matric head in the unsaturated zone and the hydrostatic pressure-head in the saturated zone), θ is the volumetric water content, t is time, and $C(= d\theta/d\psi)$ is the water capacity function defined as the gradient of the soil water retention curve. A semi-infinite sloping domain is assumed, and the upslope portion is used for the calculation here. Thus, we analyze runoff discharge that flows downslope across the vertical profile of the domain at horizontal distance (L) from the upslope end. This assumption at the downslope end was chosen to avoid local influences of specific boundary conditions such as seepage faces. The local influences of the boundary condition may be important, but our first priority is evaluation of the pure effects of soil properties and macropores without local disturbances.

As the surface boundary condition, rainfall with a constant intensity (f) was applied to the sloping domain. Overland flow occurs when the pressure reaches zero. Because

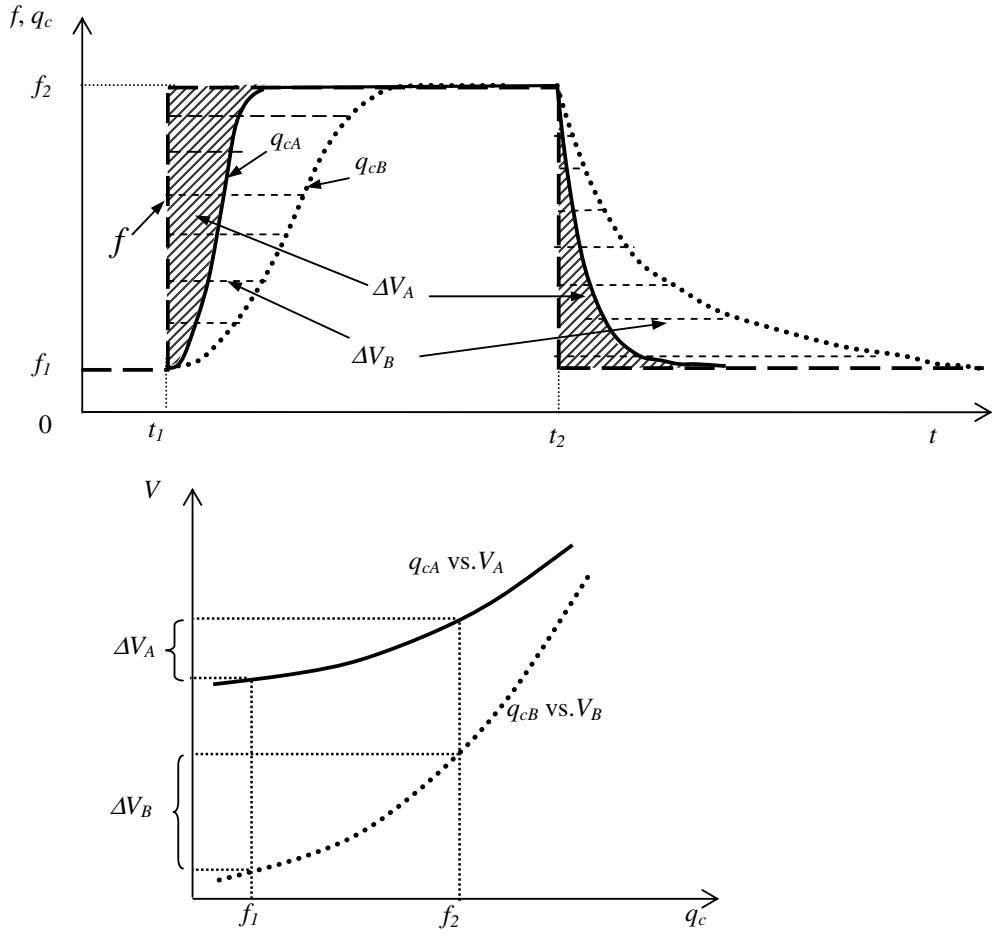

Figure 1 Schematic of a water budget during a cyclic process in response to rainfall increases and decreases (upper) and the relationship of storage change to runoff change between two steady states (lower).

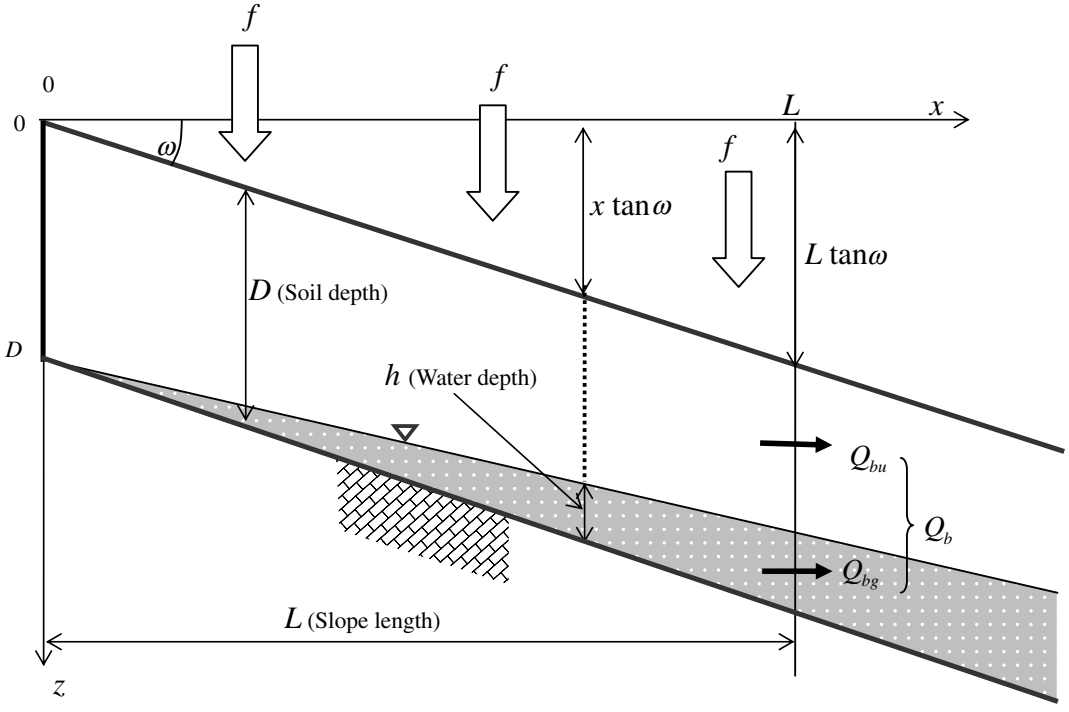

Figure 2 Schematic view of a sloping permeable domain for which a two-dimensional form of the Richards equation is applied.

Hortonian overland flow (Horton, 1939) is unusual on forested slopes, we only consider saturation overland flow (Dunne and Black, 1970) in this study. The boundary condition along the slope surface is written as

$$q_z = f \quad \text{when} \quad \psi < 0 \quad \text{at} \quad z = x\tan\omega \quad x \geqslant 0, \tag{7}$$

where ω is the slope gradient. When ψ reaches zero, the constant pressure condition (ψ = 0) is imposed to calculate saturation overland flow. As other boundary conditions, we assumed that no water flow occurs along the bottom of the permeable domain or across the upslope end. Accordingly,

$$q_z\cos\omega = 0 \quad \text{at} \quad z = x\tan\omega + D \quad x \geqslant 0, \tag{8}$$

$$q_x = 0 \quad \text{at} \quad x = 0 \quad 0 \leqslant z \leqslant D, \tag{9}$$

where D is the depth of the permeable domain. The integrated runoff discharge Q_b across the vertical profile of the domain at horizontal distance L from the upslope end is downslope flow consisting of unsaturated and saturated components, i.e., Q_{bu} and Q_{bg} (Fig. 2). These are defined as

$$Q_{bu} = \int_{L\tan\omega}^{L\tan\omega+D-H} q_x|_{x=L}\,dz, \tag{10}$$

$$Q_{bg} = \int_{L\tan\omega+D-H}^{L\tan\omega+D} q_x|_{x=L}\,dz, \tag{11}$$

$$Q_b = Q_{bu} + Q_{bg} = \int_{L\tan\omega}^{L\tan\omega+D} q_x|_{x=L}\,dz, \tag{12}$$

where H is the water depth at $x = L$. When saturation overland flow occurs, vertical flux across the surface becomes smaller than rainfall intensity. Therefore, overland flow (Q_s) can be calculated by the following equation

$$Q_s = fL - \int_0^L q_z|_{z=x\tan\omega}\,dx \tag{13}$$

Because we can assume that overland flow reaches the downslope end much faster than downslope flow does, the total runoff discharge passing across the downslope end (Q_l) is defined as

$$Q_l = Q_b + Q_s. \tag{14}$$

A Crank–Nicholson finite difference scheme was used to solve the fundamental Eq. (6) (Kosugi, 1997b).

Soil physical properties

To solve Eq. (6), we must know the functional relationships of volumetric water content and hydraulic conductivity to the matric head. Many equations have been proposed for these relationships; we selected equations that would reduce the number of parameters involved in our examination of runoff responses. We chose the physically based equation sets of Kosugi (1996, 1997a,b) derived from log-normal soil pore distributions. Kosugi (1996) defined soil water retention as

$$\theta = \theta_r + (\theta_s - \theta_r)G\left[\frac{\ln(\psi/\psi_m)}{\sigma}\right] \quad \text{for} \quad \psi < 0,$$

$$\theta = \theta_s \quad \text{for} \quad \psi \geqslant 0, \tag{15}$$

where θ_s and θ_r are the saturated and residual volumetric water contents, respectively, and G is the complementary normal distribution function defined as

$$G(y) = (2\pi)^{-0.5}\int_y^\infty \exp\left(\frac{-u^2}{2}\right)du, \tag{16}$$

and ψ_m is the median matric head corresponding to the median pore radius; σ is the standard deviation of the log-transformed soil pore radius ($\sigma > 0$), which characterizes the width of the pore-size distribution. Kosugi (1997a) expressed saturated hydraulic conductivity as a function of ψ_m and σ

$$K_s = B\frac{\exp(\sigma^2)}{\psi_m^2}. \tag{17}$$

The value of the constant B was empirically estimated to be $10^{0.4}$ cm^3 s^{-1} from data sets of soil hydraulic properties (Kosugi, 1997a). Kosugi combined that value with an equation by Mualem (1976) for permeability reduction in the unsaturated zone and gave the function of hydraulic conductivity as

$$K_0 = K_s\left[G\left\{\frac{\ln(\psi/\psi_m)}{\sigma}\right\}\right]^{1/2} \times \left[G\left\{\frac{\ln(\psi/\psi_m)}{\sigma} + \sigma\right\}\right]^2 \quad \text{for} \quad \psi < 0,$$

$$K_0 = K_s \quad \text{for} \quad \psi \geqslant 0, \tag{18}$$

where K_0 is the hydraulic conductivity given by Kosugi's equation; this is distinguished from the K used in our fundamental Eq. (6) which does include the effect of macropores as described in section 'Parameterization of the macropore effect'. Because ψ_m can be replaced by K_s using the relationship in Eq. (17), we can reduce the number of parameters to four, namely, θ_s, θ_r, K_s, and σ.

Parameterization of the macropore effect

Although many observational studies have demonstrated the important roles of macropores in rainfall-runoff responses, quantitative evaluation of macropore effects remains difficult mainly because of their heterogeneous spatial distribution (e.g., Sivapalan, 2003). To assess this effect, we applied a modification of the hydraulic conductivity function near saturation. Mohanty et al. (1997) reported a field-averaged function including the presence of preferential flow phenomena near saturation based on measurements in an agricultural field. These data are only one example, but this function may conveniently represent a typical change in the flow-governing process between capillary- and non-capillary-dominated phenomena. In addition, Brooks et al. (2004) showed that hillslope-scale lateral saturated hydraulic conductivity estimated by hydrometric observations was much larger than that obtained from a soil sample. Therefore, we offer the following approximation of the hydraulic conductivity function based on Mohanty et al.'s (1997) result:

$$K(\psi) = K_0(\psi) \quad \text{for} \quad \psi < \psi_t,$$

$$K(\psi) = \varepsilon^{\frac{\psi-\psi_t}{-\psi_t}} \times K_0(\psi) \quad \text{for} \quad \psi_t \leqslant \psi < 0,$$

$$K(\psi) = \varepsilon \times K_0(0) = \varepsilon \times K_s \quad \text{for} \quad \psi \geqslant 0, \tag{19}$$

where ε is the ratio of the saturated hydraulic conductivity considering the effect of macropores (K) to that calculated

by Eq. (17) (K_s), and ψ_t is the minimum pressure-head at which the effect of the non-capillary-dominated process appears. The thin solid curve for $K_s = 1 \times 10^{-4}$ cm s^{-1}, $\sigma = 0.8$, $\varepsilon = 50$, and $\psi_t = -10$ cm roughly agrees with the result measured by Mohanty et al. (1997) (Fig. 3). The thick solid curve for $\varepsilon = 1$ shows the relationship with no macropore effect. We can regard our method for the macropore effect as one of the parameterizations because the effect of macropores heterogeneously distributed within the domain is replaced by an enlargement effect of the hydraulic conductivity given as a homogeneous parameter in the domain. The effect of macropores is controlled by ε and ψ_t, but we assumed that the role of ε is dominant and that ψ_t can be fixed at -10 cm for our calculations using the Richards equation.

Storage volume and control parameters

Integration of the solution of our fundamental Eq. (6) over a permeable domain gives the storage volume V per unit slope length as

$$V = \frac{1}{L}\int_0^L \int_{X\tan\omega}^{X\tan\omega+D} \theta \, dz dx. \qquad (20)$$

Because the runoff rate per unit slope length Q_l/L is equal to the supplied rainfall intensity f in a steady-state, we can evaluate the runoff-buffering potential through the runoff—storage relationship; the potential is large when the increase in V is large for a given increase in f.

The parameters of our fundamental Eq. (6) that are needed for evaluation of the runoff—storage relationship are summarized as follows. Soil physical properties include

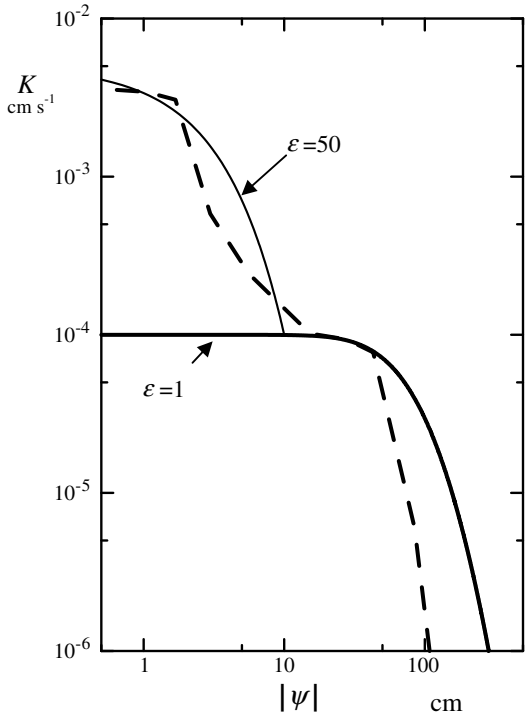

Figure 3 An example of a soil hydraulic conductivity function involving macropores. The dashed line is from measurements by Mohanty et al. (1997). The solid lines are calculated by Eq. (19).

θ_s (saturated volumetric water content), θ_r (residual volumetric water content), K_s (saturated hydraulic conductivity), and σ (standard deviation of the log-transformed soil pore radius). Slope topographic properties are L (horizontal length of the sloping domain), D (vertical depth of the domain), and ω (slope gradient). The effect of macropores is represented by ε (the ratio of the saturated hydraulic conductivity considering the effect of macropores to that calculated by Eq. (19) and ψ_t (the minimum pressure-head at which the effect of the non-capillary-dominated process appears).

Hydraulic characteristics

Distributions of pressure and hydraulic heads in a steady-state

To evaluate the effects of soil physical properties and macropores on the runoff—storage relationship of a sloping permeable domain, we first focus on the spatial distributions of hydraulic quantities as steady-state solutions of the Richards equation (Eq. (6)) because these quantities strictly control both the runoff and storage values. Therefore, it is important to investigate the spatial distribution of hydraulic quantities obtained as solutions in the steady-state. The left-hand side of Fig. 4 shows three examples of solutions from Eq. (6). The top and bottom figures in each example demonstrate the contours of pressure-head (ψ) and hydraulic head (φ), respectively. In the three examples, the common parameters have values of $\theta_s = 0.6445$, $\theta_r = 0.429$, $K_s = 0.0025$ cm s^{-1}, $\sigma = 1.4$, $D = 1$ m, $L = 10$ m, and $\omega = 30°$. The values for θ_s and θ_r are typical for forest soils, as reported by Kosugi (1999). A value for slope length smaller than that under usual field conditions was selected for illustration purposes. In each figure, a dotted line shows the water table of saturated downslope flow.

Example (A) in Fig. 4 presents distributions of ψ and φ in response to a low f value (=0.045 mm h^{-1}) as a runoff rate in a long no-rainfall period. A saturated zone is not generated within at least an L of 10 m, showing that the flow vector in the unsaturated zone is directed downslope. This low runoff rate suggests that only unsaturated downslope flow running in the downslope direction plays a role in water movement within the domain. Examples (B) and (C) illustrate runoff responses to a high f value (=4.5 mm h^{-1}) in a period with long continuous rainfall. Saturated downslope flow developed for each. However, the effect of macropores in (C) is $\varepsilon = 10$, and the macropore effect is non-existent ($\varepsilon = 1$) in (B). The water table reaches the domain surface near the downslope end in example (B), but it is very low even at the downslope end in example (C) because of the large drainage capacity of the saturated downslope flow derived from the tenfold larger effective saturated hydraulic conductivity in Eq. (19). The contours of φ in both examples seem to have two characteristics. Contours in the saturated and unsaturated zones near the groundwater table are characterized by lines perpendicular to the slope; in the upper unsaturated zone, however, contours are horizontal, indicating downslope flow vectors in the former but vertical flow in the latter. The results of examples (B) and (C) for a high runoff rate suggest that when the water table is low, rainwater with

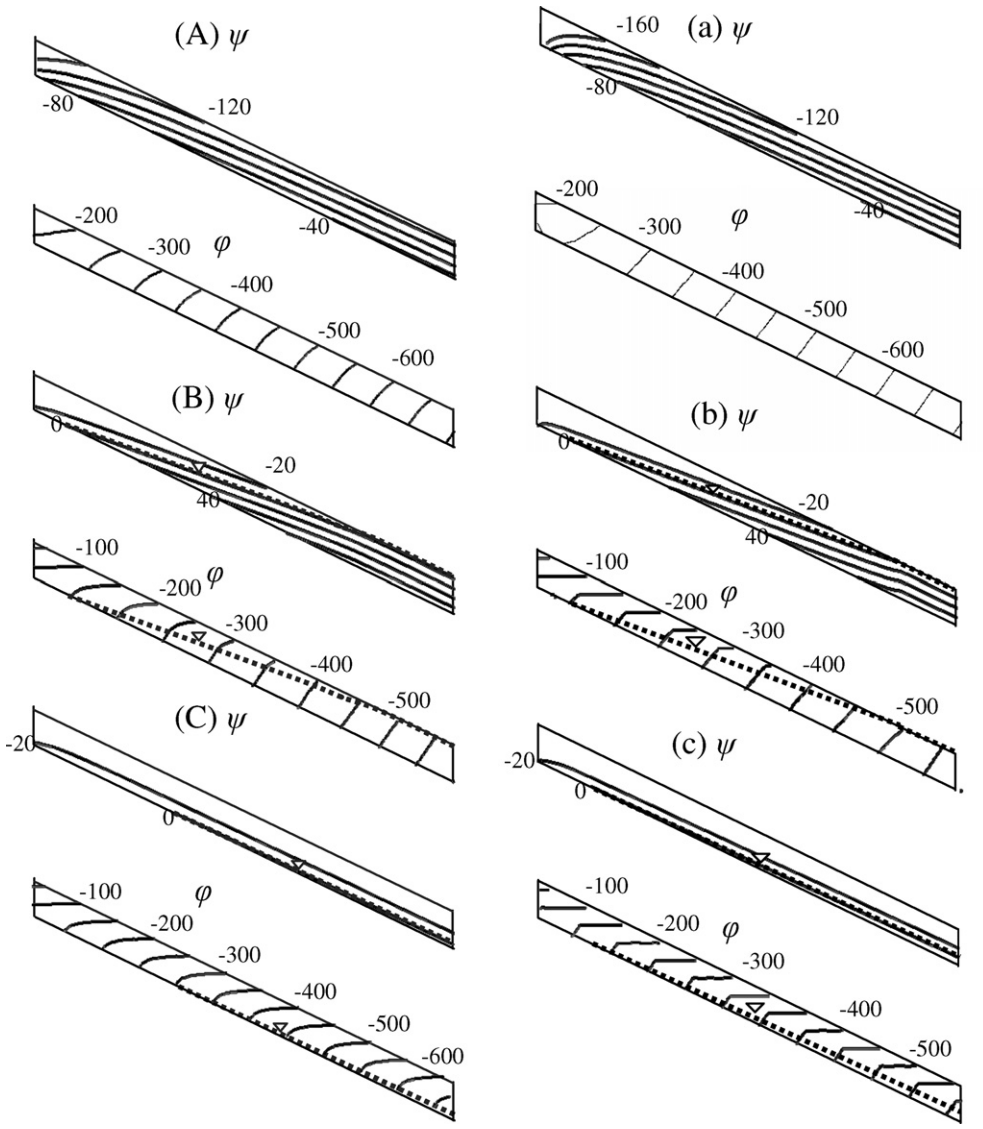

Figure 4 Typical spatial distributions of ψ and φ within a sloping domain under steady-state conditions. The left-hand figures are calculated by the Richards equation, and the right-hand figures are approximated by Eqs. (21) and (22). (A and a) $f = 0.045$ mm h^{-1}, $\varepsilon = 1$; (B and b) $f = 4.5$ mm h^{-1}, $\varepsilon = 1$ and (C and c) $f = 4.5$ mm h^{-1}, $\varepsilon = 10$.

constant intensity infiltrates vertically within the upper unsaturated zone but turns in the downslope direction near and within the saturated zone.

Approximation of pressure- and hydraulic-head distributions

The two kinds of distributions of hydraulic head yielding the vertical and downslope flow vectors in Fig. 4 suggest that steady-state pressure-head distributions can be approximated as simple schemes. This approximation makes it easier to understand the basic structure of the steady-state ψ distribution given as seemingly complex solutions of the Richards Eq. (6).

Based on the Appendix A, we can approximate the distribution of ψ in the vertical cross-section as two zones. The upper zone has a constant value of ψ_f (Eq. (A9)), and the profile in the lower zone follows Eq. (A4). Hence, we can write the distribution of ψ in these two zones using the local height measured from the domain bottom defined in Eq. (A6) as

$$\psi = \psi_b - z_c \cos^2 \omega \quad \text{for} \quad z_c \leqslant \frac{\psi_b - \psi_f}{\cos^2 \omega}, \tag{21}$$

$$\psi = \psi_f \quad \text{for} \quad z_c > \frac{\psi_b - \psi_f}{\cos^2 \omega}. \tag{22}$$

In our approximation of the steady-state pressure-head distributions, we assume that the effect of macropores on hydraulic conductivity can be neglected in the transition zone near saturation ($\psi_t \leqslant \psi < 0$ in Eq. (19)). This assumption is introduced to simplify evaluation of the macropore effect on the buffering potential. It holds that the non-capillary effects by macropores appear only in the range of positive pressure-head. Therefore, the $K - \psi$ function in our assumption is simpler than that in Eq. (19) and can be given as follows:

$$K(\psi) = K_0(\psi) \quad \text{for} \quad \psi < 0,$$
$$K(\psi) = \varepsilon \times K_0(0) = \varepsilon \times K_s \quad \text{for} \quad \psi \geqslant 0. \tag{23}$$

On the other hand, because we are considering a steady-state, the total rate of downslope flow (Q_x) draining through the vertical cross-section of the domain located at a horizontal distance (x) from the upslope end must equal the integrated rainfall rate supplied to the domain surface between the upslope end and this cross-section. Accordingly,

$$Q_x \equiv \int_0^D q_x dz_c = fx. \tag{24}$$

As described above, within both the saturated zone and part of the unsaturated zone where the flow stream lines are approximately parallel to the slope (and the contours of φ are approximately perpendicular to the slope), Darcy's law allows the following approximation for the water flow component to the x direction (q_x)

$$q_x = K(\psi) \sin\omega \cos\omega. \tag{25}$$

Within the unsaturated zone where the flow stream lines are approximated vertically, however, the flow can be directed vertically, and the x-direction flow can be neglected as

$$q_x = 0. \tag{26}$$

Fig. 5 presents schematic distributions of steady-state pressure-head and flow directions (top figure) and the relationships of the bottom and surface pressure-head values to the horizontal distance (x) (bottom figure). This shows that in the downslope zone, where $\psi_b - \psi_f \geqslant D\cos^2\omega$, the flow direction is parallel to the slope within the entire vertical profile, but in the upslope zone where $\psi_b - \psi_f < D\cos^2\omega$, the flow direction is vertical in the upper portion of the vertical profile. Therefore, in the downslope portion of the domain, Q_x is given as the integration of q_x from the bottom to the surface:

$$Q_x = fx = \int_0^D K(\psi = \psi_b - z_c\cos^2\omega)\, dz_c \times \sin\omega\cos\omega \quad \text{for} \quad \psi_b - \psi_f > D\cos^2\omega. \tag{27}$$

In the upslope portion, however, the integration is limited to the lower portion indicated by $z_c \leqslant (\psi_b - \psi_f)/\cos^2\omega$. Hence,

$$Q_x = fx = \int_0^{(\psi_b-\psi_f)/\cos^2\omega} K(\psi = \psi_b - z_c\cos^2\omega)\, dz_c \times \sin\omega\cos\omega \quad \text{for} \quad \psi_b - \psi_f \leqslant D\cos^2\omega. \tag{28}$$

In both Eqs. (26) and (27), ψ_b is the only unknown variable against a given horizontal distance x. For this reason, ψ_b can be calculated inversely from x because the integral in Eqs. (26) and (27) monotonically increases with ψ_b.

Our approximation results (Eqs. (21) and (22)) for the distributions of ψ and φ in examples (A–C) in the left side of Fig. 4 are, respectively, illustrated on the right side as (a–c). Fig. 4 demonstrates good agreement between the results of the Richards equation and the approximation for each of the three examples. There is a slight difference between the results of the two methods, resulting from the ψ values around the border between the region where stream lines are parallel to the slope and the region where they are vertical. This transition zone between the two regions exists in the results of the Richards equation, but

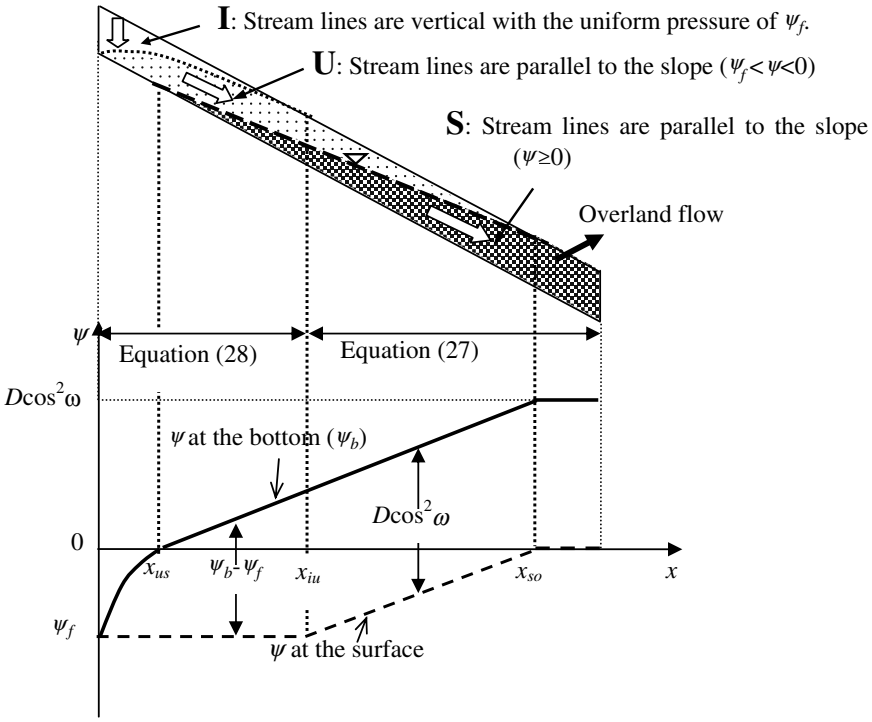

Figure 5 Schematic view of steady-state pressure-head distribution (upper) and relationships of the bottom and surface pressure-head values to the horizontal distance (x) (lower). I, infiltration zone; U, unsaturated downslope flow zone and S, saturated downslope flow zone.

the two regions share a border in the corresponding approximation. This disagreement can account for the angular φ contours for the approximations compared to the rounder φ contours of the Richards equation in examples (A–C) in Fig. 4.

Classification of the pressure-head distribution

From the considerations above, we can classify three zones of pressure-head distribution within the permeable domain (Fig. 5): (1) the region where stream lines are vertical with a uniform pressure-head of ψ_f (Eq. (22)) constitutes the infiltration zone (I zone), (2) the region where stream lines are parallel to the slope with unsaturated pressure values ($\psi = \psi_b - z_c \cos^2\omega$ in Eq. (21) but $\psi_f < \psi < 0$) is the unsaturated downslope flow zone (U zone), and (3) the region where stream lines are parallel to the slope with saturated pressure values ($\psi = \psi_b - z_c \cos^2\omega$ in Eq. (21) but $\psi \geqslant 0$) is the saturated downslope flow zone (S zone).

The horizontal distances x_{iu}, x_{us}, and x_{so} for the end point of the I zone, the start point of S zone, and the start point of saturation overland flow are defined as shown in Fig. 5 and represented as follows. Because the total width of the U and S zones described as $(\psi_b - \psi_f)/\cos^2\omega$ is just equal to D at $x = x_{iu}$, the end point of the I zone, substituting this relation into Eq. (26) yields

$$f x_{iu} = \int_0^D K(\psi = \psi_f + (D - z_c)\cos^2\omega)\ \mathrm{d}z_c \sin\omega\cos\omega. \tag{29}$$

Therefore,

$$x_{iu} = \frac{\int_{\psi_f}^{\psi_f + D\cos^2\omega} K(\psi)\,\mathrm{d}\psi\,\tan\omega}{f}. \tag{30}$$

On the other hand, the S zone is generated from x_{us} in which $\psi_b = 0$ in Eq. (21), and elevation of the U zone at x_{us} ranges from $z_c = 0$ to $z_c = -\psi_f/\cos^2\omega$. However, the upper boundary is restricted by the domain depth D. Hence, substituting these conditions into Eqs. (28) and (27) yield the following two equations, respectively:

$$f x_{us} = \int_0^{-\psi_f/\cos^2\omega} K(\psi = -z_c\cos^2\omega)\ \mathrm{d}z_c \sin\omega\cos\omega \quad \text{for} \quad \psi_f \geqslant -D\cos^2\omega, \tag{31}$$

$$f x_{us} = \int_0^{D} K(\psi = -z_c\cos^2\omega)\ \mathrm{d}z_c \sin\omega\cos\omega \quad \text{for} \quad \psi_f < -D\cos^2\omega. \tag{32}$$

These equations indicate that the magnitude of the relationship between ψ_f and $-D\cos^2\omega$ is important for our classification of the I and U zones. Therefore, a dimensionless number α is defined here as

$$\alpha = -\frac{D\cos^2\omega}{\psi_f}. \tag{33}$$

The respective values of x_{us} for Eqs. (30) and (31) are written reflecting the range of α as

$$x_{us} = \frac{\int_{\psi_f}^{0} K(\psi)\mathrm{d}\psi\,\tan\omega}{f} \quad \text{for} \quad \alpha \geqslant 1, \tag{34}$$

$$x_{us} = \frac{\int_{-D\cos^2\omega}^{0} K(\psi)\mathrm{d}\psi\,\tan\omega}{f} \quad \text{for} \quad \alpha < 1. \tag{35}$$

Finally, saturation overland flow is generated from x_{so} in which the total downslope flow in the S zone is equal to Q_x. Similar to an example by Ogden and Watts (2000),

$$x_{so} = \frac{D\varepsilon K_s \sin\omega\cos\omega}{f}. \tag{36}$$

When $\alpha = 1$, $\psi_f + D\cos^2\omega = 0$ in Eq. (32). Accordingly, the sequence of x_{iu} and x_{us} can be described from Eqs. (29), (33), and (34) as

$$x_{us} > x_{iu} \quad \text{for} \quad \alpha < 1, \tag{37}$$

$$x_{us} = x_{iu} \quad \text{for} \quad \alpha = 1, \tag{38}$$

$$x_{us} < x_{iu} \quad \text{for} \quad \alpha > 1. \tag{39}$$

Fig. 6 schematically illustrates the distributions of the I, U, and S zones with the occurrence area of saturation overland flow for each category of these equations. This figure indicates what zones appear at a given horizontal point. For example, a trilaminar structure consisting of the I, U, and S zones is only created between x_{us} and x_{iu} under the condition that $\alpha > 1$.

Fig. 7 shows relationships of x_{iu}, x_{us}, and x_{so} for a semi-infinite sloping domain to the steady-state runoff rate f. The parameter values except for the slope length are the same as those in Fig. 4, but $\varepsilon = 1$ for Fig. 7a and b, while $\varepsilon = 10$ for Fig. 7c. The value of α calculated by Eq. (33) is also plotted against f in Fig. 7d. Fig. 7a summarizes the composition of the I, U, and S zones and the occurrence area of

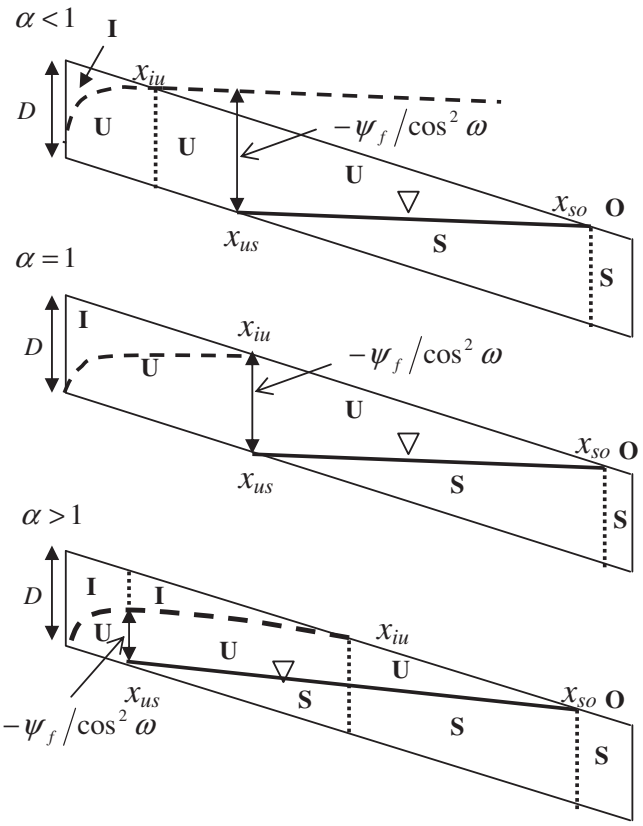

Figure 6 Schematic view of distribution patterns of the I, U, and S zones and the occurrence area of saturation overland flow categorized by Eqs. (36)–(38).

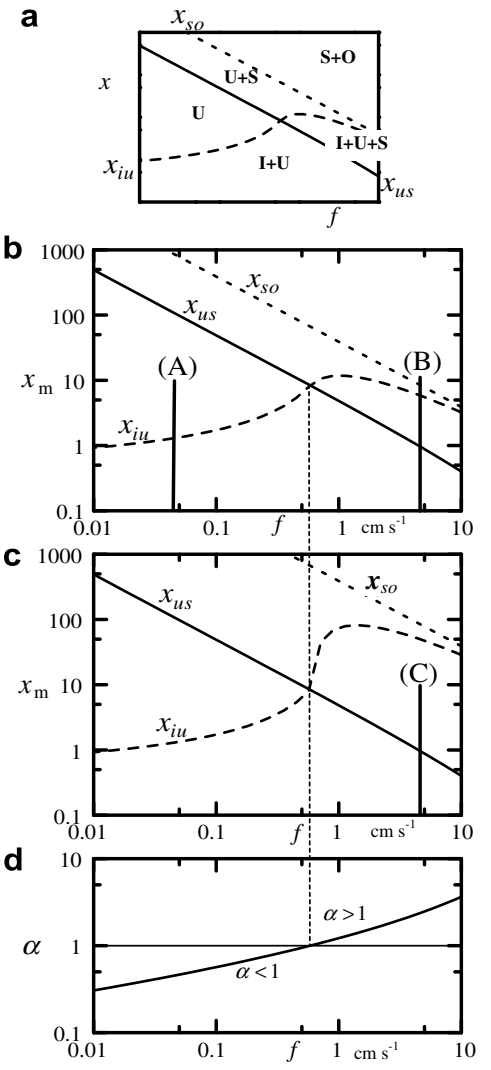

Figure 7 Relationship of horizontal distances (x_{iu}, x_{us}, and x_{so}) characterizing the zone partition to the steady-state runoff rate (f). (a) Composition of the I, U, and S zones and area of saturation overland flow (represented by 'O') for K_s = 0.0025 cm s^{-1} and $\varepsilon = 1$, (b) x–f relationship for K_s = 0.0025 cm s^{-1} and $\varepsilon = 1$, (c) x–f relationship for K_s = 0.0025 cm s^{-1} and $\varepsilon = 10$, and (d) relationship of α to f.

saturation overland flow (represented by 'O') partitioned by x_{iu}, x_{us}, and x_s, but Fig. 7b and c focus on $f - x$ relationships for each ε value. This comprehensively demonstrates what zones appear at a given horizontal distance along the slope under a steady-state when a runoff rate is provided.

In Fig. 7b and c for $\varepsilon = 1$ and 10, the both start points of S zone (x_{us}) and saturation overland flow (x_{so}) move upslope with increasing f. However, the end point of the I zone (x_{iu}) shows a more complex response. When α decreases with f (Fig. 7d), the uniform pressure value of ψ_f in the I zone decreases to large negative values (Eq. (32)). A sharp decrease of K with ψ_f (Eq. (18)) in the numerator of Eq. (29) causes x_{iu} to decrease in Fig. 7b regardless of the decrease in denominator f, and most of the domain ($x \geqslant x_{iu}$) is covered by the U zone (Fig. 7a). This pattern is included in the range of Eq. (36) and is represented by the vertical bar (A) in Fig. 7b. This coincides with example (A) in Fig. 4 for L = 10 m and f = 0.045 mm h^{-1}, where most of the sloping domain is covered with the U zone except for a short upslope portion with the I and U zones. When α increases with f (Fig. 7d), ψ_f increases, approaching zero (Eq. (32)), and the S zone appears in the downslope portion ($x \geqslant x_{us}$). For α values larger than unity, a trilaminar structure with the I, U, and S zones forms between x_{us} and x_{iu}. However, because $\psi_f + D\cos^2\omega > 0$ for $\alpha > 1$ (Eq. (32)), $K(\psi)$ reaches a constant value of K_s in the range of $0 \leqslant \psi \leqslant \psi_f + D\cos^2\omega$. Hence, increase of the numerator in Eq. (29) in response to increasing f becomes sluggish, and x_{iu} decreases in response to increase in the denominator f (Fig. 7b). This balance between the numerator and the denominator in Eq. (29) accounts for the non-monotonic relationship of x_{iu} with the maximum in Fig. 7b. A vertical bar (B) in Fig. 7b coinciding with example (B) in Fig. 4 shows the following compositions: a bilayer structure of the I and U zones near the upslope end, a trilaminar structure of the I, U, and S zones in the slope center, a bilayer structure of the U and S zones, and a full saturation of the domain with generation of saturation overland flow near the downslope end.

Fig. 7c shows similar relationships to Fig. 7b but with a macropore effect ($\varepsilon = 10$). Large differences between the figures are found in x_{iu} for $\alpha > 1$ and in x_{so}. Because it is assumed that the macropore effect only increases the water flow rate in the saturated zone (Eq. (23)), the increase of the S zone is reduced. The reduction of the S zone causes an increase in x_{iu} through decreasing the local height of the boundary between the U and I zones although the start point of the S zone x_{us} is not changed. Reduction of S zone also results in an increase in x_{so}. A vertical bar (C) in Fig. 7c coincides with example (C) in Fig. 4 and shows that the trilaminar structure covers the domain until the downslope end because of the increase in x_{iu}.

Partitioning a sloping permeable domain into I, U, and S zones demonstrates that solutions of the Richards equation under the steady-state are characterized by a simple structure that helps clarify which components play roles in the buffering potential of runoff response.

Runoff-buffering potential

Runoff–storage relationship

Fig. 8 shows examples of the relationship between the total water storage volume per unit horizontal length (V) within the domain (Eq. (20)) and the runoff rate (f) in steady states. The plots were calculated by the Richards equation, Eq. (6), using common parameter values of θ_s = 0.6445, θ_r = 0.429, σ = 1.4, D = 1 m, L = 100 m, and ω = 30°. These values are the same as those in Fig. 4 of section 'Distributions of pressure and hydraulic heads in a steady-state' except for a longer slope length representing the typical field range. The three values of saturated hydraulic conductivity (K_s) used here (0.025, 0.0025, and 0.00025 cm s^{-1}) roughly cover soil physical properties from sandy to clayey soils. The macropore effect was not given for the three as $\varepsilon = 1$, but an additional result with a macropore effect of $\varepsilon = 10$ was calculated for the case of K_s = 0.0025. The approxi-

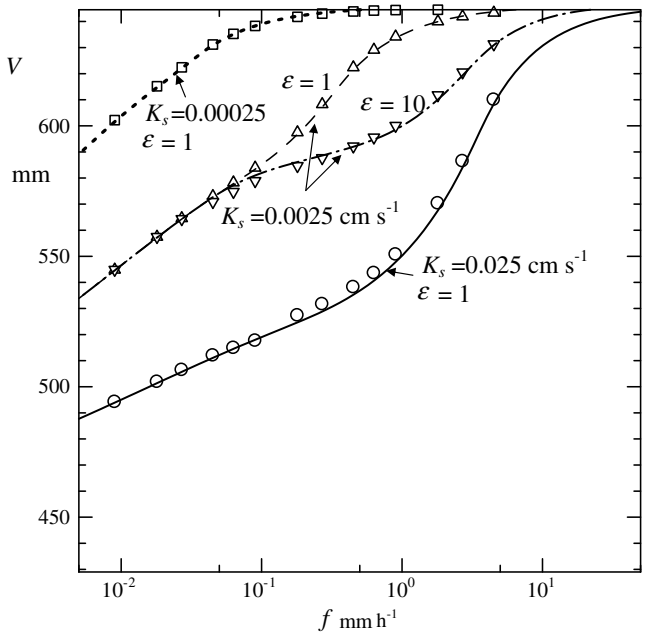

Figure 8 Relationships of the storage volume in a unit horizontal length (V) to the steady-state runoff rate (f). Symbols are calculated by the Richards equation, and lines are calculated by Eqs. (21) and (22).

mated water storage volume per unit slope length (V) based on the spatial distribution of pressure-head calculated by Eqs. (21) and (22) in section 'Approximation of pressure- and hydraulic-head distributions' is also shown in Fig. 8. This figure demonstrates that the approximations satisfactorily explain the results of the Richards equation.

For all examples in Fig. 8, V increases with f, but the relationship between V and f depends on the parameter values. The increase in V is large in the range of high f values (f > 1 mm h^{-1}) for the case of K_s = 0.025, but very small or almost zero when K_s = 0.00025. For the case of K_s = 0.0025, there is a large increase in V in the middle range of f values, and the f range shifts to a higher range for the case with macropore effects. The results indicate that the runoff-buffering potential is generally high for soils with high K_s values and that the existence of macropores contributes to shifting the f range with a high buffering potential to a higher range.

Contribution of hydraulic characteristics to runoff-buffering potential

The spatial distributions of hydraulic quantities such as pressure-head ψ and volumetric water content θ in response to each of the runoff rates f control the partitioning of the domain into the I, U, and S zones and the location of saturation overland flow. The points x_{us}, x_{iu}, and x_{so} are regarded as important indicators of partitioning as described in section 'Classification of the pressure-head distribution'. Let us examine contributions of the I, U, and S zones to the runoff-buffering potential using Fig. 9, which is the same as Fig. 8 but focusing on the zone partitioning. Calculation results with ε = 1 are referred to as C1, C2, and C3 for K_s = 0.025, 0.0025, and 0.00025 cm s^{-1}, respectively, and the result for ε = 10 and K_s = 0.0025 is referred to as C4. As shown in Fig. 7a, the unsaturated I and U zones cover the entire domain for $x_{us} > L$, and saturation overland flow occurs for $x_{so} < L$, whereas the water table of saturated downslope flow increases without overland flow in the range from $x_{us} = L$ to $x_{so} = L$. To check influences of the distributions of hydraulic quantities on runoff–storage relationships, values of f giving the relationships of $x_{us} = L$ (inversely calculated in Eqs. (33) and (34)) and $x_{so} = L$ (calculated in Eq. (35)) are marked as f_{us} and f_{so}, respectively, and the storage increases between them are represented by V_s in Fig. 9. The additional subscript in each variable (f_{us}, f_{so}, and V_s) indicates each calculation, C1–C4. Soil with K_s = 0.025 cm s^{-1} (case C1 in Fig. 9) has a high ψ_m value (=−26.7 cm) in Eq. (17) and is characterized by low soil water retention represented by sandy soil. This character yields small volumetric water content in the U zone compared to other soils because the distribution there is approximated from the hydrostatic equilibrium distribution as described in Eq. (A4). This small storage volume in the U zone accounts for a large storage increase with the rise in the water table in response to increasing f from f_{us} to f_{so} (Fig. 9). Therefore, there is a large storage increase in high-permeability soil in the range of f accompanied by a rising water table. In contrast, the relatively large storage volume in the U zone in each of the other cases (C2–C4) yields a smaller storage increase in response to increasing f. Certainly, lower ψ_m values (i.e., −84.5 cm in cases C2 and C4, and −267 cm in case C3) characterize high storage in the U and I zones even when the water table is low or non-existent. In all four cases, storage increases are small for $f \geqslant f_{so}$ because the downslope portion of the domain is fully saturated. In the range of $f < f_{us}$, where the S zone disappears, the storage increase for soil with a low K_s is

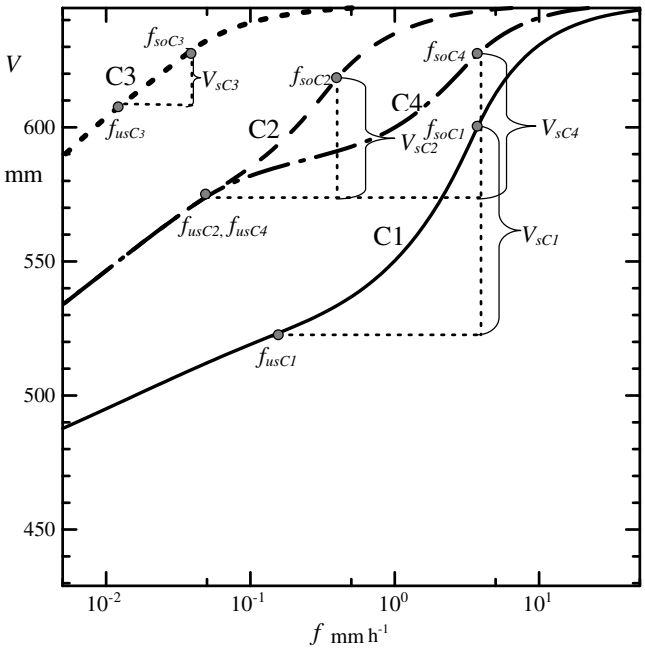

Figure 9 Relationships of the storage volume in a unit horizontal length (V) to the steady-state runoff rate (f) with zone-partitioning indicators calculated in Eqs. (33)–(35).

larger than that for soil with a high K_s. This indicates that soil with a low permeability has a relatively large storage increase in the range of the low runoff rate where the S zone is not created.

In case C4 with a macropore effect ($\varepsilon = 10$), the storage increase is similar to that in case C2 without the macropore effect, but the occurrence of saturation overland flow is drastically shifted to a higher runoff range. Thus, macropores functioned to reserve the buffering potential for higher runoff ranges and to reduce saturation overland flow. Details in macropore effects on the buffering potential are continuously discussed in the next section.

Relationship between macropore effects and soil-hydraulic properties

A previous study by Kosugi (1999) discussed the runoff-buffering potential for a vertical column, introducing the concept of water-storage capacity (see section 'Runoff–storage relationship as an indicator of runoff-buffering potential'). This index was based on water storage in a steady-state in response to constant rainfall and was basically derived from the pressure-head that can vertically transport rainwater with a constant intensity by gravitational force. Therefore, the near-surface zone of the column is covered with a constant pressure-head ψ_f as explained in section 'Approximation of pressure- and hydraulic-head distributions', and the reflected volumetric water content θ_f can be obtained by substituting Eq. (A9) into the soil physical properties of Eqs. (15) and (18) as

$$f = K = K_s\left[\frac{\theta_f - \theta_r}{\theta_s - \theta_r}\right]^{1/2} \times \left[G\left\{G^{-1}\left(\frac{\theta_f - \theta_r}{\theta_s - \theta_r}\right) + \sigma\right\}\right]^2 \qquad (40)$$

where G^{-1} is the inverse function of G (complementary normal distribution function) in Eq. (16). The θ value at the bottom of the permeable column is the saturated content θ_s because the boundary condition $\psi = 0$ is used to permit the free drainage from the bottom as given in Kosugi's (1999) study. Therefore, the water content θ in the column is distributed from θ_f near the surface to zero at the bottom, and the water storage index can be calculated from the vertical distribution of θ. A further consideration is added here. If the column depth D is very large, most of the column is occupied by the water content of θ_f except the near-bottom portion. Water storage asymptotically approaches $D\theta_f$ with increasing D. When the column is infinitely deep, the relationship of storage to the runoff rate, which is equal to the rainfall intensity f at a steady-state, is approximately reduced to the simple relationship f–$D\theta_f$ derived from an intrinsic hydraulic property, the K–θ relationship in Eq. (39), independent of topographic properties.

This character of a vertical soil column is reflected in the I zone of the two-dimensional domain that we analyzed. Fig. 10 is similar to Figs. 8 and 9 but the f–V relationships are for $K_s = 0.0025$ cm s^{-1} with various macropore effects of $\varepsilon = 1$, 10, 100, and 1000. Fig. 10 also shows the f–$D\theta_f$ relationship calculated by Eq. (39). This figure clearly demonstrates that the f–V relationship asymptotically approaches the f–$D\theta_f$ relationship with increasing ε. This tendency is explained by the high drainage capacity of the S zone caused by macropore effects. When the capacity

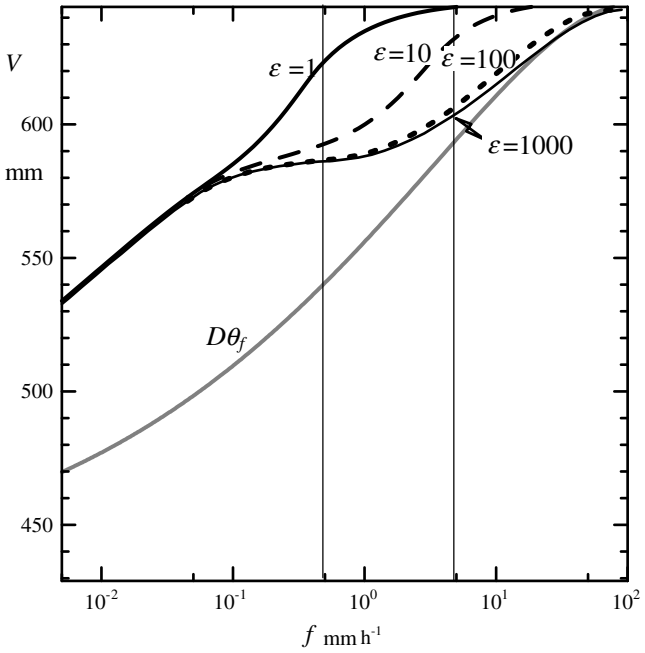

Figure 10 Relationships of the storage volume in a unit horizontal length (V) to the steady-state runoff rate (f) for various macropore effects ($\varepsilon = 1$, 10, 100, and 1000) for $K_s = 0.0025$ cm s^{-1}. A thick gray line indicates the f–$D\theta_f$ relationship calculated by Eq. (39).

becomes large with ε increasing, the water table is suppressed even for high f values. In addition to the low water table of the S zone, the width of the U zone, given as $-\psi_f/\cos^2\omega$ from the definition of the U zone in section 'Classification of the pressure-head distribution', also becomes small because ψ_f rises to a near-zero value for high f values. These lead to expansion of the I zone with constant values of ψ_f and θ_f. Therefore, the runoff-buffering potential follows the intrinsic hydraulic property of the K–θ relationship when the domain includes many macropores contributing to the high drainage capacity of downslope flow in the S zone. Some hydrometric observations on hillslopes have provided evidence that ψ measured at shallow depths during rainfall events reflects the intrinsic hydraulic property (Tani, 1997; Torres et al., 1998).

To compare the buffering potential for each of the various cases of macropore effects, we consider the storage increase in response to a given increase in f. For example, Fig. 10 illustrates an increase in f from 0.5 mm h^{-1} to 5 mm h^{-1}. Because the f_{so} value for $\varepsilon = 1$ is 0.49 (Fig. 9), saturation overland flow occurs near the downslope end even for $f = 0.5$ mm h^{-1}, and the storage increase responding to the increase in f to 5 mm h^{-1} is suppressed by the limitation of the depth of the permeable domain. Hence, the storage increase in this case without macropore effects is smaller than that in the case where $\varepsilon = 10$. On the other hand, the storage increases for cases with large macropore effects of $\varepsilon = 100$ and 1000 are also smaller than the increase for $\varepsilon = 10$ (Fig. 10). These cases with low buffering potentials are caused by high drainage capacities of the S zone. Therefore, there exists an ε value giving the maximum storage increase responding to a given runoff increase and that both

low and high macropore effects result in low storage increases. We can conclude that a moderate magnitude of the macropore effect may provide a high runoff-buffering potential.

Summary and concluding remarks

One of the most basic characteristics of runoff discharge is whether the shape of a hydrograph is stable or flashy in response to given rainfall and evapotranspiration conditions. This characteristic is referred to as the runoff-buffering potential. Because the runoff–storage relationship of a runoff system generally controls this potential, we proposed an assessment method involving investigation of the effects of each system property on the runoff–storage relationship under steady-state conditions. A one-dimensional vertical column and a two-dimensional sloping domain were considered in the assessment of our method. That investigation showed that the buffering potential of the vertical column basically originated from intrinsic soil hydraulic properties independent of topography. Although this character is only strictly satisfied for a hypothetical infinitely deep column, it reflects the sloping domain as a zone in which the flow stream lines are vertical. This zone was called the I zone and distinguished from the U and S zones in which flow directions are parallel to the slope.

The runoff-buffering potential of the sloping domain was assessed with the classification consisting of the I, U, and S zones. A high potential represented by a large storage increase in the runoff–storage relationship occurs for soil with high permeability, particularly in the range of runoff rate accompanied by a rising water table, although soil with low permeability has a relatively large storage increase in the range of low runoff rate without a saturated zone. The existence of macropores shifts the range of large storage increases to high runoff rates and contributes to the reduction of saturation overland flow. As a result, there is a moderate magnitude of the macropore effect giving the maximum increase in storage in response to a given increase in runoff.

This study has examined runoff-buffering potential by analyzing the dependency of storage on the runoff rate under steady-state conditions. While a steady-state is rare under field conditions, this basic assumption is considered necessary because the spatial-distribution characteristics of hydraulic quantities obtained from the fundamental equation have not yet been clarified for saturated and unsaturated flow even under a steady-state. Seibert et al. (2003) discussed the interaction between unsaturated and saturated zones and classified it into cases in which these zones are positively and negatively correlated. Duffy (1996) considered water balance equations for both an unsaturated flow system and a saturated flow system and revealed that a competitive relation exists between unsaturated and saturated storages. Such an interaction or a competition between saturated and unsaturated zones can be systematically represented by our classification of the I, U, and S zones. The runoff discharge from the sloping domain is produced directly from the U and S zones, whereas the rainfall as a surface boundary condition controls the I zone. These steady-state characteristics may provide insight into the dynamics of unsteady states as well. Such an extended application of the classification will be conducted in further studies.

The present paper has focused on introducing the methodology and classifying the hydraulic quantities in steady states. The effects of properties on runoff-buffering potential were only discussed based on some calculation examples. Evaluation of effects through sensitivity analyses will be presented in future papers using dimensionless similarity parameters.

Acknowledgements

I am grateful to Dr. Ken'ichirou Kosugi of the Graduate School of Agriculture, Kyoto University, for providing the numerical solution of a two-dimensional form of the Richards equation and for his kind suggestions regarding the methodology of this study.

Appendix A. Derivation of approximated pressure- and hydraulic-head distributions in a steady-state

Fig. A1 illustrates an approximated distribution of φ along a vertical cross-section on a sloping domain. Generally, groundwater flow within an aquifer on a steep slope, such as our saturated downslope flow on a hillslope, is approximated by an extended Dupuit–Forchheimer assumption whereby flow lines are parallel to the slope (Beven, 1981). This indicates that the contours of φ are perpendicular to the slope. We can extend the assumption of parallel stream lines from the saturated zone to the unsaturated zone where φ contours are still perpendicular to the slope in the three examples in Fig. 4. Within the saturated or unsaturated zone, the vertical profiles of ψ and φ can be approximated in reference to the illustration at the right side of Fig. A1. The values of ψ and φ at two points, P_1 and P_2, on a vertical cross-section are related with the assistance of P_3, the intersection of a line parallel to the slope through P_1, and a line perpendicular to the slope through P_2 such that

$$\psi_2 - z_2 = \varphi_2 = \varphi_3 = \psi_3 - z_3 = \psi_1 - z_3, \tag{A1}$$

where the suffix coincides with the point number. From Eq. (A1), we can obtain the following relations for ψ and φ between P_1 and P_2:

$$\psi_2 = \psi_1 - z_3 + z_2 = \psi_1 + (z_2 - z_1)\cos^2\omega, \tag{A2}$$

$$\varphi_2 = \psi_2 - z_2 = \psi_1 + (z_2 - z_1)\cos^2\omega - z_2 = \varphi_1 - (z_2 - z_1)\sin^2\omega. \tag{A3}$$

Therefore, the profiles of φ and ψ along the vertical cross-section are approximately written as

$$\psi = \psi_b - z_c\cos^2\omega, \tag{A4}$$

$$\varphi = \varphi_b + z_c\sin^2\omega, \tag{A5}$$

where ψ_b and φ_b are ψ and φ at the bottom of the permeable domain, respectively, and z_c is the local height measured upward from the domain bottom, which is defined as

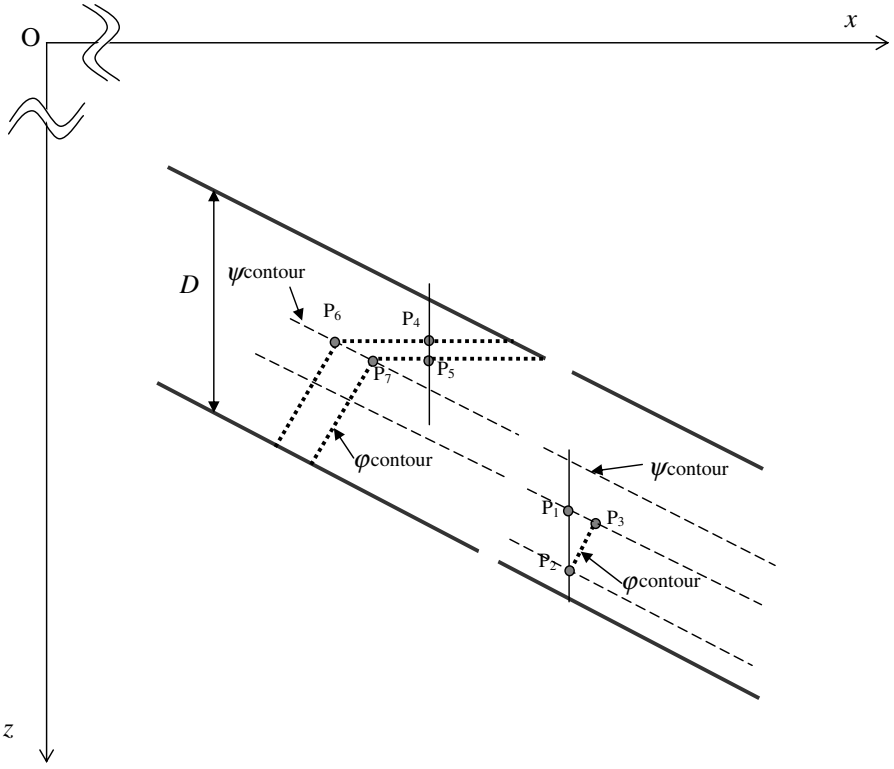

Figure A1 Schematic view of the approximated contours of ψ and φ under steady-state conditions. The dashed and dotted lines are the contours of ψ and φ, respectively.

$$z_c = X\tan\omega + D - z. \tag{A6}$$

Next, we approximate vertical ψ distributions in the zone where slope-perpendicular φ contours turn horizontal (see the left side of Fig. A1). Consider a vertical cross-section in the zone where φ contours are horizontal, and draw a horizontal line from each of the two points (P_4 and P_5) on this cross-section. The intersections of these horizontal lines and the upper-boundary contour of ψ, below which the ψ contours are parallel to the slope, are marked as P_6 and P_7, respectively. P_6 and P_4 are located on a φ contour, and P_7 and P_5 are on another φ contour such that

$$\varphi_6 = \varphi_4, \quad \varphi_7 = \varphi_5. \tag{A7}$$

The elevations of P_6 and P_7 are the same as those of P_4 and P_5, respectively, and P_6 and P_7 are located on the contour of ψ:

$$\psi_5 = \psi_7 = \psi_6 = \psi_4. \tag{A8}$$

As a result, ψ has an approximately constant value within the zone where φ contours are horizontal.

Recall that we are considering the ψ distribution under a steady-state derived from our surface boundary condition with a constant rainfall intensity (f). Substituting $q_z = f$ into Eq. (4) gives the following simple relationship because $\partial\psi/\partial z = 0$ within the zone of a constant pressure-head value:

$$f = K(\psi_f). \tag{A9}$$

This zone is covered with a constant ψ_f value calculated inversely from the rainfall intensity by the function in Eq. (A9), consisting of Eqs. (17) and (18). The classic study by Rubin and Steinhardt (1963) found such a distribution for vertical infiltration from constant rainfall intensity. Our result indicates that this pattern may be extended to the portion of the unsaturated zone where φ contours are horizontal in the sloping domain. For example (A) in Fig. 4, ψ_f is -166 cm for $f = 0.045$ mm h^{-1}, and for examples (B) and (C), ψ_f is -32.0 cm for $f = 4.5$ mm h^{-1}. The distributions of ψ within the upper unsaturated zone at the upslope portion in example (B) and the upper unsaturated zone for the entire slope in example (C) show good agreement for the ψ_f value of -32.0 cm in Fig. 4, whereas ψ within the upper zone at the upslope portion in example (A) shows a slightly higher value.

References

Anderson, S.P., Dietrich, W.E., Montgomery, D.R., Torres, R., Conrad, M.E., Loague, K., 1997. Downslope flow paths in a steep unchanneled catchment. Water Resour. Res. 33, 2637–2653.

Beven, K., 1981. Kinematic downslope flow. Water Resour. Res. 17, 1419–1424.

Beven, K., Kirkby, M.J., 1979. A physically based, variable contributing area model of basin hydrology. Hydrol. Sci. Bull. 24, 43–69.

Bradshaw, C.J.A., Sodhi, N.S., Peh, K.S.H., Brook, B., 2007. Global evidence that deforestation amplifies flood risk and severity in the developing world. Global Change Biol. 13, 2379–2395.

Brooks, E.S., Boll, J., McDaniel, P.A., 2004. A hillslope-scale experiment to measure lateral saturated hydraulic conductivity. Water Resour. Res. 40, W04208. doi:10.1029/2003WR00285.

Calder, I.R., 1999. Blue Revolution, Land Use and Integrated Water Resources Management. Earthscan, London, 192pp.

Duffy, C.J., 1996. A two-state integral-balance model for soil moisture and groundwater dynamics in complex terrain. Water Resour. Res. 32, 2421–2434.

Dunne, T., Black, R.D., 1970. An experimental investigation of runoff production in permeable soils. Water Resour. Res. 6, 478–490.

Fan, Y., Bras, R.L., 1998. Analytical solutions to hillslope subsurface storm flow and saturation overland flow. Water Resour. Res. 34, 921–927.

Freeze, A., 1972. Role of subsurface flow in generating surface runoff: 2. Upstream source areas. Water Resour. Res. 8, 1272–1283.

Fukushima, Y., 1988. A model of river flow forecasting for a small forested mountain catchment. Hydrol. Process. 2, 167–185.

Grip, H., Fritsch, J.M., Bruijnzeel, L.A., 2004. Soil and water impacts during forest conversion and stabilisation to new land use. In: Bonell, M., Bruijnzeel, L.A. (Eds.), Forests, Water and People in the Humid Tropics. Cambridge University Press, Cambridge, pp. 561–589.

Hayashi, Y., Kosugi, K., Mizuyama, T., 2006. Changes in pore size distribution and hydraulic properties of forest soil resulting from structural development. J. Hydrol. 331, 85–102.

Holmes, M.G.R., Young, A.R., Gustard, A., Grew, R., 2002. A region of influence approach to predicting flow duration curves within ungauged catchments. Hydrol. Earth Syst. Sci. 6, 721–731.

Horton, R.E., 1939. The interpretation and application of runoff-plat experiments with reference to soil erosion problems. Proc. Soil Sci. Soc. Am. 3, 340–349.

Kao, C., Zimmer, D., Bouarfa, S., 2001. Steady state analysis of unsaturated flow above a shallow water-table aquifer drained by ditches. J. Hydrol. 250, 122–133.

Katsuyama, M., Ohte, N., Kabeya, N., 2005. Effects of bedrock permeability on hillslope and riparian groundwater dynamics in a weathered granite catchment. Water Resour. Res. 41, W01010. doi:10.1029/2004WR00327.

Kitahara, H., Terajima, T., Nakai, Y., 1994. Ratio of pipe flow to through flow. J. Jpn. For. Soc. 76, 10–17 (in Japanese with English summary).

Kosugi, K., 1996. Lognormal distribution model for unsaturated soil hydraulic properties. Water Resour. Res. 32, 2697–2703.

Kosugi, K., 1997a. New diagrams to evaluate soil pore radius distribution and saturated hydraulic conductivity of forest soil. J. For. Res. 2, 95–101.

Kosugi, K., 1997b. Effect of pore radius distribution of forest soils on vertical water movement in soil profile. J. Jap. Soc. Hydrol. Water Resour. 10, 226–237.

Kosugi, K., 1999. New index to evaluate water holding capacity of forest soils. J. Jpn. For. Soc. 81, 226–235 (in Japanese with English summary).

Kosugi, K., Katsura, S., Katsuyama, M., Mizuyama, T., 2006. Water flow processes in weathered granitic bedrock and their effects on runoff generation in a small headwater catchment. Water Resour. Res. 42, W02414. doi:10.1029/2005WR00427.

Lee, D.H., 2007. Testing a conceptual hillslope recession model based on the storage–discharge relationship with the Richards equation. Hydrol. Process. 21, 3155–3161.

Mohanty, B.P., Bowman, R.S., Hendrickx, J.M.H., van Genuchten, M.Th., 1997. New piecewise-continuous hydraulic functions for modeling preferential flow in an intermittent flood-irrigated field. Water Resour. Res. 33, 2049–2063.

Montgomery, D.R., Dietrich, W.E., 2002. Runoff generation in a steep, soil-mantled landscape. Water Resour. Res. 38, 1168. doi:10.1029/2003WR00249.

Mualem, Y., 1976. A new model for predicting the hydraulic conductivity of unsaturated porous media. Water Resour. Res. 12, 513–522.

Ogden, F.L., Watts, B., 2000. Saturated area formation on nonconvergent hillslope topography with shallow soils: a numerical investigation. Water Resour. Res. 36, 1795–1804.

Rubin, J., Steinhardt, R., 1963. Soil water relations during rain infiltration (I) Theory. Proc. Soil Sci. Soc. Am. 27, 246–251.

Seibert, J., Rodhe, A., Bishop, K., 2003. Simulating interactions between saturated and unsaturated storage in a conceptual runoff model. Hydrol. Process. 17, 379–390.

Shimizu, T., 1980. Relation between scanty runoff from mountainous watershed and geology, slope and vegetation. Bull. For. For. Prod. Res. Inst. 310, 109–128 (in Japanese with English summary).

Sivapalan, M., 2003. Process complexity at hillslope scale, process simplicity at the watershed scale: is there a connection? Hydrol. Process. 17, 1037–1041.

Smettem, K.R.J., Chittleborough, D.J., Richards, B.G., Leaney, F.W., 1991. The influence of macropores on runoff generation from a hillslope soil with a contrasting textural class. J. Hydrol. 122, 235–252.

Sugawara, M., 1995. Tank model. In: Singh, V.J. (Ed.), Computer Models in Watershed Hydrology. Water Resources Publications, CO, USA, pp. 165–214.

Tani, M., 1997. Runoff generation processes estimated from hydrological observations on a steep forested hillslope with a thin soil layer. J. Hydrol. 200, 84–109.

Dietrich, R., Torres, W.E., Montgomery, D.R., Anderson, S.P., Loague, K., 1998. Unsaturated zone processes and the hydrologic response of a steep, unchanneled catchment. Water Resour. Res. 34 (8), 1865–1879.

Troch, P.A., Paniconi, C., van Loon, E.E., 2003. The hillslope-storage Boussinesq model for downslope flow and variable source areas along complex hillslopes: 1. Formulation and characteristic response. Water Resour. Res. 39 (11), 1316. doi:10.1029/2002WR00172.

Tsutsumi, D., Sidle, R.C., Kosugi, K., 2005. Development of a simple lateral preferential flow model with steady state application in hillslope soils. Water Resour. Res.. doi:10.1029/2004WR00387.

Uchida, T., Kosugi, K., Mizuyama, T., 2001. Effects of pipeflow on hydrological process and its relation to landslide: a review of pipeflow studies in forested headwater catchments. Hydrol. Process. 15, 2151–2174.

Zaslavski, D., Sinai, G., 1981. Surface hydrology: III. Causes of lateral flow. J. Hydraul. Eng.- ASCE 107 (HY1), 37–52.